Optimization of Spin-Triplet Supercurrent in Ferromagnetic Josephson Junctions

Carolin Klose, Trupti S. Khaire, Yixing Wang, W. P. Pratt, Jr., and Norman O. Birge*
Department of Physics and Astronomy, Michigan State University, East Lansing, Michigan 48824-2320, USA

B. J. McMorran, T. P. Ginley,† J. A. Borchers, B. J. Kirby, B. B. Maranville, and J. Unguris
National Institute of Standards and Technology, Gaithersburg, Maryland 20899, USA
(Received 18 August 2011; published 20 March 2012)

We have observed long-range spin-triplet supercurrents in Josephson junctions containing ferromagnetic (F) materials, which are generated by noncollinear magnetizations between a central Co/Ru/Co synthetic antiferromagnet and two outer thin F layers. Here we show that the spin-triplet supercurrent is enhanced up to 20 times after our samples are subject to a large in-plane field. This occurs because the synthetic antiferromagnet undergoes a ''spin-flop'' transition, whereby the two Co layer magnetizations end up nearly perpendicular to the magnetizations of the two thin F layers. We report direct experimental evidence for the spin-flop transition from scanning electron microscopy with polarization analysis and from spin-polarized neutron reflectometry. These results represent a first step toward experimental control of spin-triplet supercurrents.

DOI: 10.1103/PhysRevLett.108.127002 PACS numbers: 74.50.+r, 74.20.Rp, 74.45.+c, 75.70.Cn

Experimental and theoretical progress in superconducting/ferromagnetic (S/F) hybrid systems has been impressive over the past decade [1]. When a conventional spin-singlet Cooper pair crosses the S/F interface, the two electrons enter into different spin bands in F with different Fermi wave vectors [2]. The resulting oscillations in the pair correlation function lead to oscillations in several observable quantities [1], but unfortunately the oscillations decay exponentially as soon as the F-layer thickness exceeds the electron mean free path [3].

In contrast to spin-singlet electron pairs, spin-triplet pairs can survive in F as long as they would in a normal metal. While spin-triplet superconductivity arises only rarely in bulk materials [4], it was predicted a decade ago that such pairs can be induced in S/F hybrid systems in the presence of certain kinds of magnetic inhomogeneity involving noncollinear magnetizations [5–7]. Experimental evidence for such spin-triplet pairs was elusive for many years [8,9]; then, in 2010, several groups published convincing evidence for spin-triplet supercurrent in S/F/S Josephson junctions containing only conventional spin-singlet S materials [10–13]. The conversion from spin-singlet to spin-triplet pairs was accomplished either by introducing magnetic inhomogeneity artificially, or by relying on a source of inhomogeneity intrinsic to the materials in the samples. In our Josephson junctions, the central F layer is in fact a Co/Ru/Co ''synthetic antiferromagnet'' (SAF) with the magnetizations of the two Co layers locked antiparallel to each other by a strong exchange field mediated by the Ru layer (see Fig. 1). We insert additional thin ferromagnetic F′ layers on either side of the SAF; these extra layers are crucial to the creation of spin-triplet pairs inside the junctions [14].

What happens when one tries to magnetize the junctions by applying a large in-plane magnetic field? After magnetization, contrary to expectations, the critical current, I_c, increases up to a factor of 20 relative to its value in the as-grown state. This seemingly counter-intuitive result can be understood by considering a unique property of the SAF: when the large magnetizing field $\boldsymbol{H}_{\rm app}$ is applied, the Co magnetizations ''scissor'' towards $\boldsymbol{H}_{\rm app}$. When the field is removed, the Co magnetizations relax back to directions perpendicular to $\boldsymbol{H}_{\rm app}$. This SAF ''spin-flop'' transition was predicted and first demonstrated over a decade ago [15,16].

Our sample geometry is illustrated in Fig. 1. The two layers labeled F′ are both either pure Ni or $Pd_{0.88}Ni_{0.12}$ alloy in this work [10,17]. The inner Cu layers magnetically isolate the F′ layers from the Co layers. The outer Cu layers are present for historical reasons and because Co

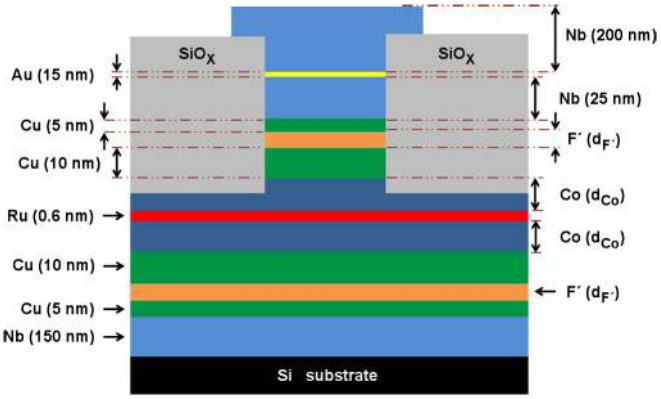

FIG. 1 (color online). Schematic diagram of the Josephson junctions used in the this work, shown in cross section.

grows better on a Nb/Cu buffer layer [18]. The entire multilayer except for the top Nb is sputtered in one run without breaking vacuum. Circular junctions with diameters of 10, 20, and 40 μm are patterned by photolithography and ion milling, followed by deposition of insulating SiO_x to isolate the top and bottom Nb leads. Finally, the top Nb electrode is sputtered through a mechanical mask. The purpose of the Au layer is to suppress oxidation of the structure during processing; at low temperature the Au becomes superconducting due to the proximity effect with the surrounding Nb layers. The Nb layers start to superconduct just above 9 K; all of the transport data presented here were obtained at 4.2 K.

The original purpose of the Co/Ru/Co SAF was to provide a strong exchange field for the electrons while simultaneously producing little to no magnetic flux in the junctions. Large-area Josephson junctions containing a strong ferromagnetic material such as Co exhibit complicated and irregular ''Fraunhofer patterns'' when subject to an applied transverse magnetic field [18,19]. The irregularities are due to a random pattern of constructive and destructive interference in the gauge-invariant phase difference across the junction caused by the complicated spatial variation of the magnetic vector potential [20]. The presence of the Ru restores textbooklike Fraunhofer patterns centered very close to zero applied field [18], an indication that there is very little intrinsic magnetic flux in the junctions. In this work, the Ru will serve a second, unexpected role, namely, to provide a simple way to force the magnetizations of the Co layers to be perpendicular to the magnetizations of the F′ layers.

As background to the new data presented here, we briefly review our previous results [10,17]. Josephson junctions of the type illustrated in Fig. 1, but without the F′ layers, exhibit a critical supercurrent (I_c) that decays rapidly with increasing total Co thickness, D_{Co} [18]. Insertion of the F′ layers with appropriate thicknesses ($d_{\mathrm{F}'}$ between 3 and 6 nm for F′ = PdNi, or $d_{\mathrm{F}'}$ between 1 and 2 nm for F′ = Ni) enhances I_c by over 2 orders of magnitude when $D_{\mathrm{Co}} = 20$ nm. The dependence of I_c on D_{Co} is nearly flat when D_{Co} varies over the range of 12–28 nm, with F′ = PdNi and $d_{\mathrm{PdNi}} = 4$ nm. This long-range behavior of the critical supercurrent is the signature of its spin-triplet nature. For the rest of this Letter we will focus on samples containing F′ layers of either PdNi or Ni, with D_{Co} fixed at 20 nm.

Figure 2 illustrates what happens when samples with F′ = Ni and four values of d_{Ni} are subjected to an applied in-plane magnetic field, H_{app}. After each value of field is applied, the full Fraunhofer pattern is remeasured in the vicinity of zero field, and we plot the maximum value of I_c at the central peak of the Fraunhofer pattern. Figure 2 shows that, at first, very little happens. Then when H_{app} exceeds the coercive field of the Ni layers (in the range of $\mu_0 H \approx 0.05$–0.15 T depending on d_{Ni}), I_c starts to increase dramatically. At large H_{app}, I_c flattens out after having increased by a large factor—up to 20 for $d_{\mathrm{Ni}} = 1.0$ nm. At the same time, the central peaks in the Fraunhofer patterns shift to a small negative field value that is proportional to the Ni thickness, and consistent with the remnant magnetization of our Ni films [21]. The Fraunhofer shifts indicate that the Ni layers are fully magnetized when I_c saturates in Fig. 2. Similar behavior to that shown in Fig. 2 was found in samples with F′ = PdNi with $d_{\mathrm{PdNi}} = 4$ nm.

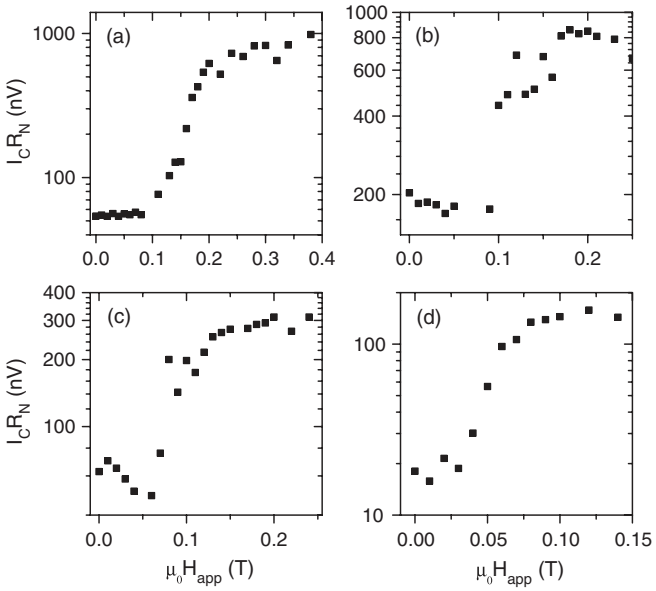

FIG. 2. Critical current times normal-state resistance (I_cR_N) measured in remanence, as a function of magnetizing field H_{app} for Josephson junctions containing F′ = Ni, for Ni thicknesses $d_{\mathrm{Ni}} = 1.0$, 1.5, 2.0, and 2.5 nm for panels (a)–(d), respectively. Magnetizing the samples enhances I_c by a large factor that depends on d_{Ni}. (Uncertainties are dominated by variations in magnetic configuration, and can be estimated from the scatter in the data.)

Theory predicts that the spin-triplet supercurrent in our samples is optimized when the magnetizations of the two F′ layers are perpendicular to those of the central Co layers [14,22,23]. In fact, no spin-triplet pairs should be generated when all the magnetizations in the sample are collinear. The large enhancement of the critical current shown in Fig. 2 strongly suggests that magnetizing the samples optimizes the orthogonality of the Co magnetizations with respect to the F′ magnetizations. The small shift of the Fraunhofer pattern, on the other hand, indicates that only the F′ layers are magnetized in the direction of $\boldsymbol{H}_{\mathrm{app}}$. This scenario is perfectly plausible in the light of the ''spin-flop'' transition of the SAF [15,16].

To identify the magnetic structure responsible for the enhancement of the spin-triplet supercurrent, we made a large-area sample of the form Si/Nb(150 nm)/Cu(10 nm)/Co(6 nm)/Ru(0.6 nm)/Co(6 nm)/Cu(10 nm),

which has the Josephson junction layer structure shown in Fig. 1 through the Cu layer on top of the upper Co layer. The Co magnetizations were characterized with the complementary techniques [24] of specular polarized neutron reflectivity (PNR) and scanning electron microscopy with polarization analysis (SEMPA) at room temperature. (PNR measurements were also performed at low temperature on a different sample, with results similar to those shown here.) PNR nondestructively measures the net in-plane magnetization for each ferromagnetic layer, even in the presence of a field. SEMPA combined with ion milling images the remanent magnetic structure in each layer.

The magnetization of the ferromagnetic layers was first analyzed in the as-grown state. For the PNR measurements, performed on the NG-1 Reflectometer at the NIST Center for Neutron Research, the spin states of the incident and scattered neutrons were selected to produce the nonspin-flip (NSF) cross sections (R^{++} and R^{--}) and the spin-flip (SF) cross sections (R^{+-} and R^{-+}) shown in Fig. 3. The NSF scattering is sensitive to the nuclear structure of the sample, and the splitting between R^{++} and R^{--} originates from the projection of the magnetization parallel to the guide field (< 0.002 T). The SF scattering is entirely magnetic and arises from the component of the magnetization that is perpendicular to the guide field. The data were all fit (solid lines in Fig. 3) to a dynamical scattering model based upon the one-dimensional wave equation using the REFL1D software package [25] to determine the depth dependence of both the chemical structure and vector magnetization averaged across the 1-cm^2 area of the sample [21].

In Fig. 3(a), the NSF cross sections are dominated by structural contributions, but the R^{++} and R^{--} exhibit a small splitting indicative of a net magnetization component parallel to the guide field. The SF scattering is small, but nonzero, consistent with a slight canting of the Co layer magnetizations away from the guide field. The diamond-head arrows in Fig. 4(a) and 4(b) represent the average orientation and magnitude of the net magnetizations of the top and bottom Co layers, 822 ± 25 emu/cm^3 at $153° \pm 10°$ and 722 ± 25 emu/cm^3 at $335° \pm 10°$ respectively [21], obtained from the PNR fits. SEMPA was then used to image the magnetization of each layer within a 1-mm^2 ion-milled window of the same sample. Ion milling with 800 eV Ar ions first reveals the top Co layer magnetization [Fig. 4(a)], and then the bottom Co layer [Fig. 4(b)]. The distribution of magnetization directions in these images are shown in the corresponding polar plots. Both the PNR and SEMPA measurements indicate a preferred direction for the magnetization in the as-grown state, with most of the magnetization aligned along an angle approximately 25° relative to a sample edge. Both measurements also show antiferromagnetic coupling between the top and bottom Co layers.

A 0.3 T field was then applied along the sample edge (at 0° in Fig. 4), and the PNR and SEMPA remanent state measurements were repeated [Figs. 3(b), 4(c), and 4(d)]. Specifically, the SEMPA images in Figs. 4(c) and 4(d), performed on another 1-mm^2 area of the sample, show that the field induces a more complicated remanent magnetic

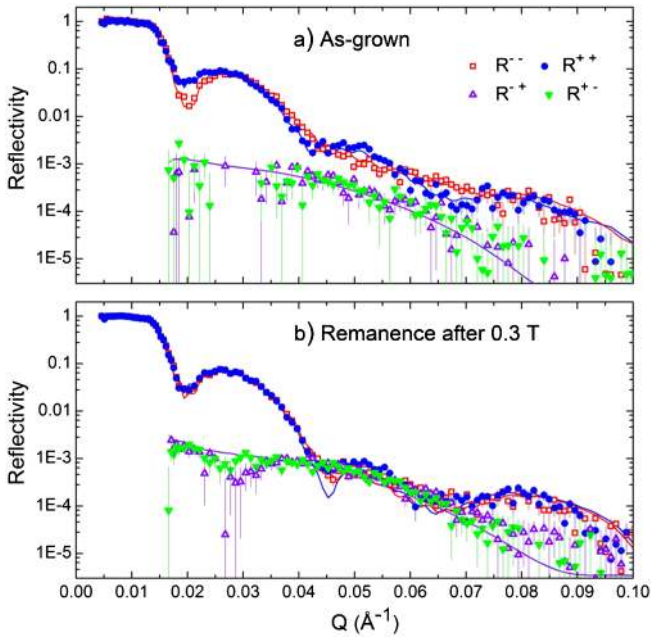

FIG. 3 (color online). Polarized neutron reflectivity data and fits (solid lines) as a function of wave vector Q from a partial Josephson junction in a guide field of <0.002 T: (a) as-grown and (b) near remanence after application of a 0.3 T field. The nonspin-flip cross sections, R^{++} and R^{--}, correspond to the solid circles and open squares, respectively. The spin-flip cross sections, R^{-+} and R^{+-}, correspond to the open and solid triangles. The error bars represent an uncertainty of $\pm 1\sigma$.

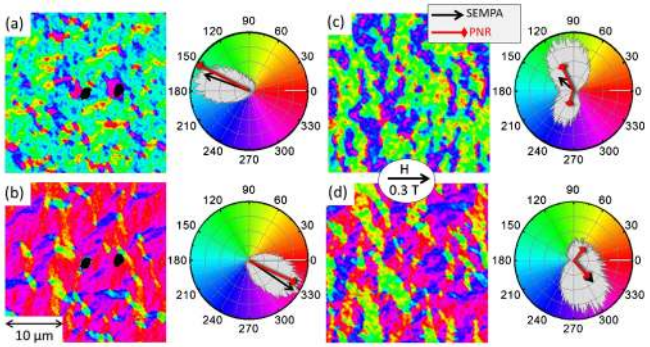

FIG. 4 (color online). SEMPA images of the magnetization in the top (a), (c) and bottom (b), (d) layers before (a), (b) and after (c), (d) an applied field of 0.3 T. Polar histograms to the right of each figure show the distribution (in grey) of magnetization angles in the image. The average magnetization from the image (standard arrow) and the magnetization measured using PNR (diamond-head arrow) are also shown. The magnitude of the small diamond-head arrows in (c) and (d), corresponding to the secondary domain state, has been scaled up by a factor of 5.

structure, with a bimodal domain distribution within each layer that is tilted away from the applied field. These SEMPA data are consistent with a relaxed scissor state induced by a spin-flop transition. The results from the PNR measurements [Fig. 3(b)] are again complementary to the SEMPA measurements. The specular reflectivity shows an increase in the SF scattering by a factor of about 1.6 at high Q relative to the as-grown state [Fig. 3(a)], indicating that the projections of the layer magnetizations perpendicular to the guide field have increased. In addition the R^{++} and R^{--} NSF cross sections are now essentially equal, consistent with a decrease in the projection of the net magnetization parallel to the guide field. Motivated by the unusual magnetic configuration revealed by SEMPA, the remanent PNR data [Fig. 3(b)] were fit with a model [21] that includes an incoherent addition of equal scattering contributions from two distinct domain states. The larger diamond-head arrows in Fig. 4(c) and 4(d), obtained from the PNR fits, represent the net Co layer magnetizations in the dominant domain state. The magnetizations of the top and bottom Co layers are 381 ± 20 emu/cm^3 at $115° \pm 10°$ and 273 ± 20 emu/cm^3 at $311° \pm 10°$, respectively. The smaller diamond-head arrows correspond to the reduced net magnetizations of 38 ± 15 emu/cm^3 at $253° \pm 20°$ and 32 ± 15 emu/cm^3 at $52° \pm 20°$, respectively, for the top and bottom Co layers in the secondary domain state. It is significant that the Co layer moments are still effectively antiferromagnetically coupled within both domains, but the net magnetizations of each layer within each of the two domains have rotated in opposite directions away from the applied field, consistent with a spin-flop transition. Note that SEMPA and PNR measurements on similar samples containing F′ layers of Ni or PdNi also confirm that the remanent magnetizations of those layers point in the direction of H_{app} after application of 0.3 T.

The PNR and SEMPA measurements reveal that the evolution of the magnetic structures within the SAF is complex, but is consistent with a spin-flop transition. While this transition qualitatively explains the field-induced spin-triplet supercurrent enhancement, it is notable that the state has multiple in-plane domains and the Co layer magnetizations are tilted from the direction perpendicular to the applied field. This complexity prevents us from predicting quantitatively the magnitude of the supercurrent enhancement from the PNR/SEMPA analysis.

In conclusion, we have observed a large enhancement of the spin-triplet supercurrent in S/F′/SAF/F′/S Josephson junctions when the F′ layers are magnetized by an applied field and the SAF undergoes a spin-flop transition. This result confirms the theoretical prediction that the spin-triplet supercurrent is maximum when the magnetizations of the adjacent ferromagnetic layers inside the junctions are aligned perpendicular to each other. This result also underscores the need for characterization and control of the magnetic structure to optimize the performance of spin-triplet S/F/S devices. This could be done in the future by a number of methods, e.g., by exploiting shape anisotropy or by using magnetic materials with perpendicular-to-plane anisotropy.

We acknowledge helpful conversations with Mark Stiles and Bob McMichael. We also thank R. Loloee and B. Bi for technical assistance, and use of the W. M. Keck Microfabrication Facility. This work was supported by the U.S. Department of Energy under Grant No. DE-FG02-06ER46341.

*birge@pa.msu.edu
†Present address: Physics Department, Juniata College, Huntingdon, PA 16652, USA.

[1] A. I. Buzdin, Rev. Mod. Phys. **77**, 935 (2005).
[2] E. A. Demler, G. B. Arnold, and M. R. Beasley, Phys. Rev. B **55**, 15174 (1997).
[3] F. S. Bergeret, A. F. Volkov, and K. B. Efetov, Phys. Rev. B **64**, 134506 (2001).
[4] A. P. Mackenzie and Y. Maeno, Rev. Mod. Phys. **75**, 657 (2003), and references therein.
[5] F. S. Bergeret, A. F. Volkov, and K. B. Efetov, Phys. Rev. Lett. **86**, 4096 (2001).
[6] A. Kadigrobov, R. I. Shekhter, and M. Jonson, Europhys. Lett. **54**, 394 (2001).
[7] M. Eschrig, J. Kopu, J. C. Cuevas, and Gerd Schön, Phys. Rev. Lett. **90**, 137003 (2003).
[8] R. S. Keizer, S. T. B. Goennenwein, T. M. Klapwijk, G. Miao, G. Xiao, and A. Gupta, Nature (London) **439**, 825 (2006).
[9] I. Sosnin, H. Cho, V. T. Petrashov, and A. F. Volkov, Phys. Rev. Lett. **96**, 157002 (2006).
[10] T. S. Khaire, M. A. Khasawneh, W. P. Pratt Jr., and N. O. Birge, Phys. Rev. Lett. **104**, 137002 (2010).
[11] J. W. A. Robinson, J. D. S. Witt, and M. G. Blamire, Science **329**, 59 (2010).
[12] D. Sprungmann, K. Westerholt, H. Zabel, M. Weides, and H. Kohlstedt, Phys. Rev. B **82**, 060505 (2010).
[13] M. S. Anwar, F. Czeschka, M. Hesselberth, M. Porcu, and J. Aarts, Phys. Rev. B **82**, 100501 (2010).
[14] M. Houzet and A. I. Buzdin, Phys. Rev. B **76**, 060504(R) (2007).
[15] J.-G. Zhu and Y. Zheng, IEEE Trans. Magn. **34**, 1063 (1998).
[16] H. C. Tong, C. Qian, L. Miloslavsky, S. Funada, X. Shi, F. Liu, and S. Dey, J. Appl. Phys. **87**, 5055 (2000).
[17] M. A. Khasawneh, T. S. Khaire, C. Klose, W. P. Pratt Jr., and N. O. Birge, Supercond. Sci. Technol. **24**, 024005 (2011).
[18] M. A. Khasawneh, W. P. Pratt Jr., and N. O. Birge, Phys. Rev. B **80**, 020506(R) (2009).
[19] O. Bourgeois, P. Gandit, J. Lesueur, A. Sulpice, X. Grison, and J. Chaussy, Eur. Phys. J. B **21**, 75 (2001).
[20] T. S. Khaire, W. P. Pratt Jr., and N. O. Birge, Phys. Rev. B **79**, 094523 (2009).
[21] See Supplemental Material at http://link.aps.org/supplemental/10.1103/PhysRevLett.108.127002 for I_c vs

H data (Fraunhofer patterns) and a detailed description of the model and procedure used to fit the PNR data.

[22] A. F. Volkov and K. B. Efetov, Phys. Rev. B **81**, 144522 (2010).

[23] L. Trifunovic and Z. Radovic, Phys. Rev. B **82**, 020505(R) (2010).

[24] J. A. Borchers, J. A. Dura, J. Unguris, D. Tulchinsky, M. H. Kelley, C. F. Majkrzak, S. Y. Hsu, R. Loloee, W. P. Pratt, and J. Bass, Phys. Rev. Lett. **82**, 2796 (1999).

[25] P. A. Kienzle, J. Krycka, N. Patel, and I. Sahin, computer software REFL1D (Version 0.6.19), University of Maryland, 2011. Available from http://reflectometry.org/danse.